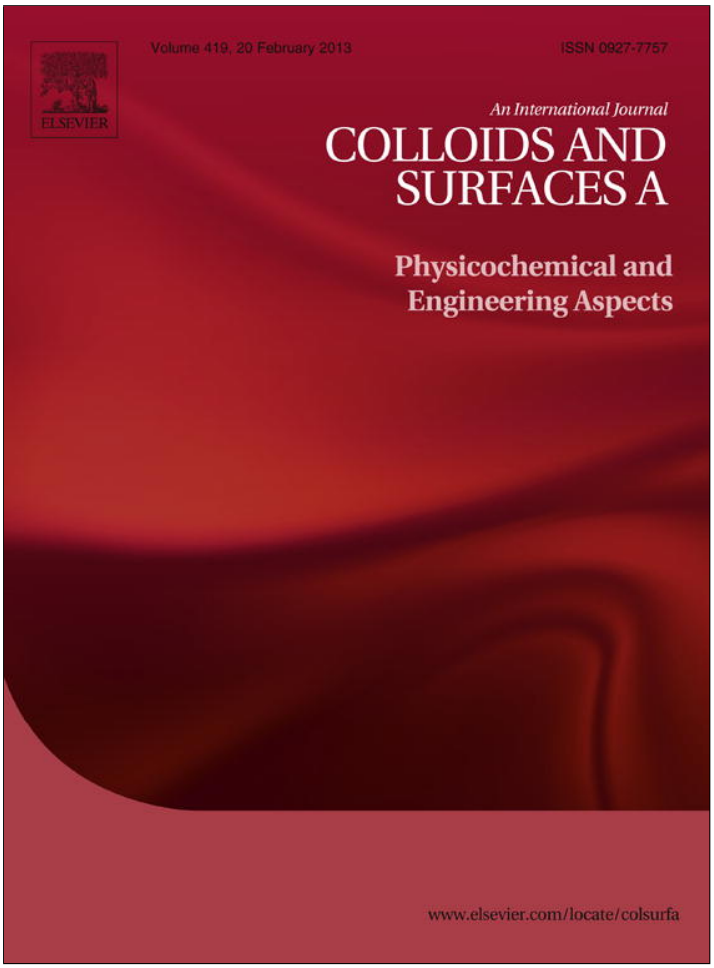

Colloids and Surfaces A: Physicochem. Eng. Aspects 419 (2013) 166–173

Contents lists available at SciVerse ScienceDirect

Colloids and Surfaces A: Physicochemical and Engineering Aspects

journal homepage: www.elsevier.com/locate/colsurfa

Effect of structure and bonding on the interfacial properties and the reactivity of layered double hydroxides and Zn hydroxide salts

Ricardo Rojas*, Carla E. Giacomelli

INFIQC-CONICET, Departamento de Fisicoquímica, Facultad de Ciencias Químicas, Universidad Nacional de Córdoba, Argentina

HIGHLIGHTS

- Correlation between structure/binding and interfacial properties/reactivity is described.
- LDHs and LHSs exhibited anion and ligand exchange reactions, respectively.
- Layers structure and chemical interactions between aromatic anions determined particle charge.
- Aromatic anions intercalation induced a hydrophobic character increase.
- The interlayer anion ionizable group influenced binding strength to LDH/LHS layers.

GRAPHICAL ABSTRACT

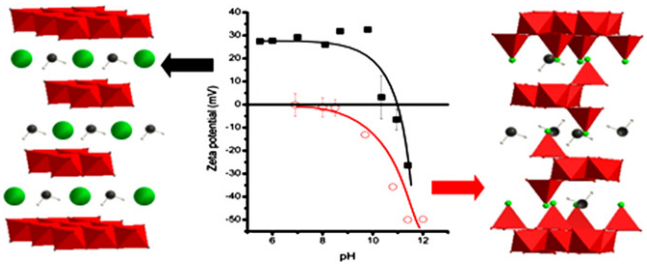

ARTICLE INFO

Article history:
Received 30 October 2012
Received in revised form
27 November 2012
Accepted 3 December 2012
Available online 11 December 2012

Keywords:
Intercalation compounds
Zeta potential
Hydrophobic/hydrophilic character
Anion/ligand exchange

ABSTRACT

Both layered double hydroxides (LDHs) and Zn layered hydroxide salts (LHSs) are intercalation compounds with potential applications as pollutant sorbents and antimicrobial, drug, and pesticide carriers, among others. Their reactivity and interfacial properties are essential to these applications and dependent on the layer structure and interlayer anion nature. In this work, the structure and bonding of Zn–Cr LDHs and Zn—LHSs intercalated with chloride, 4-chlorobenzoate, and 4-chlorobenzylsulfonate were analyzed using X-ray diffraction and infrared spectroscopy. Afterwards, their effect on interfacial properties and reactivity was assessed by zeta potential measurements, contact angle determinations, and hydroxide anions uptake. Due to their different structure, LDHs presented electrostatic interactions between their layers and the intercalated anions, while LHSs portrayed coordinated binding. The latter exhibited neutrally or negatively charged particles and ligand exchange reactions, while LDHs presented positively charged particles and anion exchange reactions. The interlayer anion nature also modulated the behavior of these solids: the introduction of aromatic anions strongly modified the hydrophilic/hydrophobic character of the surface, while their ionizable group determined the anion binding strength and consequently the anion/ligand exchange equilibrium of LDHs and LHSs.

1. Introduction

Layered double hydroxides (LDHs) and Zn-layered hydroxide salts (LHSs) are intercalation compounds with different bi-dimensional structures derived from that of brucite ($Mg(OH)_2$). The structure of this hydroxide can be described as a compact packing of hydroxide anions, where divalent ions are placed in half of the octahedral sites, resulting in layers of edge-sharing octahedrae. LDHs structure is derived by isomorphic substitution of divalent by trivalent ions in octahedral sites [1,2]. LDH layers present a positive charge excess leading to intercalation of anions that share the interlayer domain with solvent molecules (usually water). On the

* Corresponding author. Tel.: +54 3514334169; fax: +54 3514334188.
E-mail address: rrojas@fcq.unc.edu.ar (R. Rojas).

0927-7757/$ – see front matter © 2012 Elsevier B.V. All rights reserved.
http://dx.doi.org/10.1016/j.colsurfa.2012.12.002

other hand, the structure of Zn^{2+} containing LHSs (simonkolleite, for example) is derived by elimination of a quarter of Zn^{2+} ions in octahedral sites and their addition in tetrahedral sites at the bottom and top of each empty octahedron [3,4]. Three vertices of each tetrahedron are occupied by hydroxide anions of the layer, while the fourth is occupied either by the interlayer anion or by water molecules, depending on the affinity of the interlayer anion for divalent Zn^{2+}. Due to their different layer structure, LDHs possess anion exchange properties and LHSs ligand exchange capabilities and LHSs present a higher exchange sites density than LDHs [4].

LDHs and LHSs not only present exchange properties with anions in solution but also acid base reactions due to the hydroxylated nature of their layers [4,5]. These bulk properties are appealing for a wide range of applications, namely drug and gene carriers [6,7], pollutant scavengers [8,9], etc. Besides, the surface properties of these solids (particle charge [10], hydrophobic/hydrophilic character [11]) are key factors to stabilize their dispersions [12], optimize their adsorptive properties [13], or adjust their interactions with biological membranes [14], proteins [15], polymers [16], etc. Both bulk and surface properties of LDHs and LHSs are determined by two main factors: the layers structure, and the interlayer anion nature. The former has an impact on stability at acid pHs and on the exchange capacity of the solids [4,17], whereas the interlayer anion affects the exchange equilibrium constant and/or the charge and hydrophobic/hydrophilic character [11,18] of the particles.

In previous works, the influence of the interlayer anion on the surface properties and reactivity of LDHs was explored for chloride, carbonate, and dodecylsulfate [5,18,19]. In the present work, the study is extended to different layer structures and the effect of aromatic anions with different ionizable groups (carboxylate and sulfonate). LDHs (not Zn–Cr LDHs, used in this work as a model, but Mg–Al or Zn–Al LDHs) and LHSs intercalated with such anions have been proposed as sorbents of aromatic pollutants [20,21]. These solids are studied as delivery systems for drugs [22], pesticides [23], and antimicrobial agents [24] that present an aromatic moiety. Finally, they can be used for the formation of polymer nanocomposites with increased thermal stability [25] or antimicrobial activity [24].

This work aims at determining the effect of layer structure and interlayer anions on the reactivity and interfacial properties of Zn–Cr LDHs and Zn LHSs. The structure and bonding of solids intercalated with chloride and aromatic anions (4-chlorobenzoate and 4-chlorobenzylsulfonate) were analyzed using X-ray diffraction and infrared spectroscopy. Afterwards, their structure and bonding were related to the interfacial properties (zeta potential and hydrophilic character, determined by electrophoresis and contact angle determinations, respectively) and reactivity (exchange and protonation/deprotonation reactions, determined by hydroxide anions uptake and interlayer anion release vs. pH curves).

2. Experimental

All solutions were prepared with purified water (18 MΩ Milli Q, Millipore System). All chemicals were reagent grade and they were used with no previous purification. Unless otherwise stated, all experiments were performed at 25 °C.

2.1. Synthesis and structural characterization

LDHs and LHSs, containing either Cl^-, 4-chlorobenzoate (R—COO^-, R=ClC_6H_4), or 4-chlorobenzylsulfonate (R—SO_3^-, R=ClC_6H_4), were prepared by co-precipitation at constant pH [26,27]. For LDHs, a 0.1 L metal ion solution (1.0 mol L^{-1} $ZnCl_2$ and 0.5 mol L^{-1} $CrCl_3$) was added drop wise to a three-necked flask containing a 0.1 L, 1.5 mol L^{-1} sodium salt solution of the corresponding interlayer anion. The addition was performed at a constant pH (=7), fixed by addition of a 2 mol L^{-1} NaOH solution, under vigorous stirring, and in a nitrogen atmosphere to avoid carbonate intercalation. Once reactant addition was finished, the mixture was kept under stirring and pH control for 2 h. The obtained solids were then separated by centrifugation, washed with water several times, and finally dried at 60 °C. The obtained samples were denoted as LDH—Cl, LDH—COO, and LDH—SO_3 depending on the interlayer anion. For LHSs, the main differences of the synthesis procedure were the metal ion (1.25 mol L^{-1} $ZnCl_2$) and base (2.7 mol L^{-1} NH_4OH) solutions [27]. The samples obtained were denoted as LHS—Cl, LHS—COO, and LHS—SO_3.

Zn and Cr contents of the samples were determined by atomic absorption spectrometry in a PerkinElmer AA-3100 instrument. The solid was dissolved in HNO_3 and then diluted to meet the calibration range. Carbon content was determined by an Euro Elemental Analyze Eurovector instrument. Water content was assessed by thermogravimetric analysis in a SETARAM Setsys Evolution 16/18 instrument, with a 5 °C min^{-1} heating rate. Powder X-Ray diffraction (PXRD) patterns were recorded in a Phillips X'pert Pro instrument using a CuKα lamp (λ = 1.5408 Å) at 40 kV and 40 mA between 3° and 70° (2θ) in step mode (0.05°, 1.2 s). Fourier transform infrared (FT-IR) spectra were obtained from KBr pellets (1:100 sample/KBr ratio) in a FT-IR Bruker IFS28 instrument. The transmission electron microscope (TEM) images were recorded on a JEOL JSM-2010 transmission electron microscope (TEM) at an acceleration voltage of 200 kV. For TEM imaging, a droplet of the sample suspension was dropped on a copper grid coated with a carbon film.

2.2. Interfacial characterization

Hydrodynamic apparent diameter (d) and zeta potential (ζ) of the samples were determined by dynamic light scattering (DLS) and electrophoretic light scattering (ELS) respectively, in a Delsa Nano C instrument (Beckman Coulter) equipped with a 658 nm laser diode, at a 165° scattering angle. The measurements were performed in 0.01 g dispersions of the corresponding samples in 0.1 L of 5×10^{-2} mol L^{-1} NaCl solution. They were ultrasonically dispersed for 30 min and their d and ζ values were determined at different pH values, adjusted by addition of a NaOH solution. d values were obtained from the autocorrelation function ($g^{(2)}$) by the cumulant method while electrophoretic mobilities were converted to ζ using the Smoluchowski equation.

Contact angle measurements were performed by the sessile drop method using a homemade contact angle goniometer. Deionized water drops were used over pellets repared by compressing the samples powder (0.2 g) at 2 tons in a 13 mm diameter (FT-IR) die.

2.3. Reactivity

Hydroxide anions uptake (σ_{OH}) vs. pH curves [5,19] were registered in 0.1 g sample dispersions in either 5×10^{-3}, 5×10^{-2}, or 5×10^{-1} mol L^{-1} NaCl solutions (0.05 L). For R-COO^- and R-SO_3^- containing samples, the curves were also registered in 5×10^{-2} mol L^{-1} NaCl + 5×10^{-3} mol L^{-1} Na(R—COO) or Na(R—SO_3) solutions, respectively. The curves were registered using a Titrando 905 automatic titrator (Metrohm) controlled by Tiamo software and coupled to a Metrohm 9.0262.100 combined pH electrode and a Dosino 800 dosing unit. The titrant (standardized 0.1 mol L^{-1} HCl or NaOH solutions) volumes were adjusted to achieve regular pH gaps. To avoid dissolution of the samples, titrations of LDHs and LHSs were started at 5 and 8, respectively. After each titrant addition, equilibrium was considered to have been reached at a 2 mV/min electrode drift. The net σ_{OH} was calculated at each pH as the difference between total amounts of NaOH added to the dispersion and

those required to bring a blank solution to the same pH. In the case of samples containing R—COO^- or R—SO_3^- anions, a parallel experiment in 5×10^{-2} mol L^{-1} NaCl was performed where aliquots of the dispersion were taken at different pH values. After centrifugation, the concentration of the corresponding aromatic anion was determined in a Shimadzu UV1601 UV–vis spectrophotometer at 235 nm and 225 nm for R—COO^- and R—SO_3^- anions, respectively.

In order to normalize the data and allow comparison, σ_{OH} and interlayer anion release ($-\sigma_A$) were expressed in terms of surface density, calculated as:

$$\sigma = \frac{F \cdot \Gamma}{S} \quad (1)$$

where F is the Faraday constant, Γ is the net σ_{OH} /$-\sigma_A$ per unit mass and S is the total layer specific area of the corresponding sample, calculated as: $S = 3^{1/2} a^2 N/M$ [28], where a is the unit cell parameter, N is the Avogadro constant, and M is the chemical formula weight.

3. Results and discussion

3.1. Structural characterization

The chemical analyses of the samples and their theoretical chemical formulae are shown in Table 1. The formulae were calculated assuming that Zn–Cr LDH and Zn LHS layers presented a fixed layer composition ($[Zn_2Cr(OH)_6]^+$ and $[Zn_5(OH)_8]^{2+}$, respectively [27,29–31]) and that the layer charge was exclusively balanced by the expected interlayer anion. The experimental data showed very good agreement with those calculated by the proposed chemical formula (values between parentheses in Table 1), indicating that a single phase with the expected structure and interlayer anion was obtained in all cases. Accordingly, the PXRD patterns of all samples (supplementary information, Figure S1A) were indexed with a single set of cell parameters (Table 1). The unit cells of LDH—Cl and LHS—Cl were similar to those of hydrotalcite (JCPDS card 89-0460) and simonkolleite (07-0155), respectively. The interlayer anion produced significant changes in the c parameter, in good accord with the larger size of R—COO^- and R—SO_3^- anions. For LDHs, basal spacing values ($d = c/3$) were quite concordant with those obtained for other R—COO^- and R—SO_3^- intercalated LDHs [16,32,33], where the anions were assumed to be disposed in an interdigitated, tilted arrangement. LDH—COO and LDH-SO_3 patterns indicated that these samples presented lower ordering than LDH—Cl, which was in agreement with the larger anion size and weaker electrostatic interactions between the layers.

The c parameters for both LHS—COO and LHS—SO_3 were similar to that obtained for benzoate intercalated LHSs [21,34]. LHS—COO and LHS—SO_3 samples presented interlayer distances larger than those of the corresponding LDHs, ascribed to the higher charge density of LHS layers compared to LDHs [4]. As a result, the interlayer anion was more densely packed and arranged in a less tilted disposition in LHSs. Both LHS—COO and LHS—SO_3 presented diffraction patterns characteristic of highly ordered solids due to the rigid coordination bonding between the Zn^{2+} ions of the layers and the interlayer anions, [4,34] and the strong π–π stacking interactions between the densely packed aromatic anions. The different crystallinity of LDH and LHS samples also reflected in their particle shape, irregular for the former, hexagonal for the latter (Supporting information, Figure S2). However, the shape of the particles was unaffected by the interlayer anion in both cases.

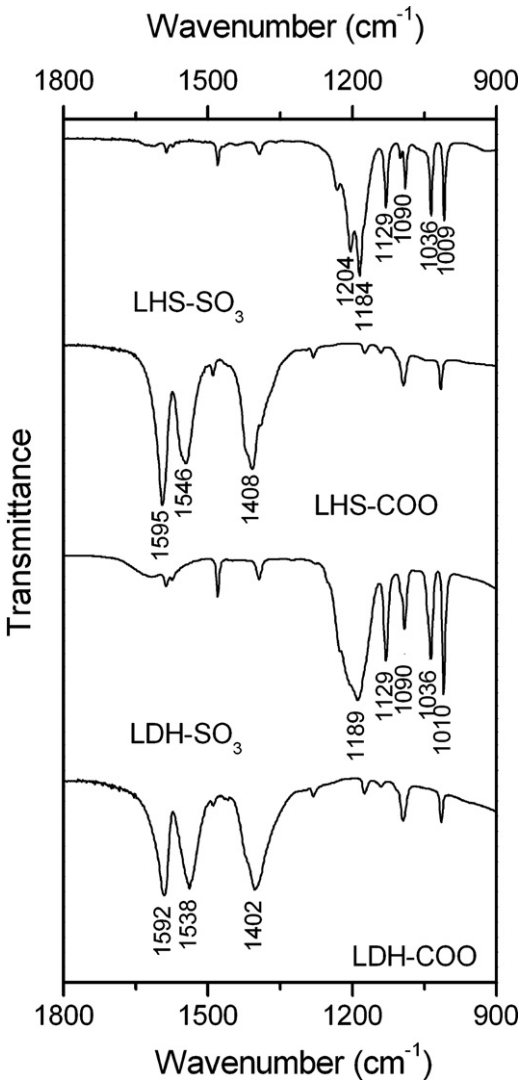

Fig. 1. FT-IR spectra of LDH and LHS samples intercalated with aromatic anions.

Binding between the charged groups of the organic anions and the host layers was studied by FT-IR spectroscopy (Fig. 1). Thus, LDH—COO and LHS—COO presented bands assigned to the ν_{asym} and ν_{sym} stretching modes of R—COO^- carboxylate group [35,36]. For LDH—COO, these bands were obtained at 1538 and 1402 cm^{-1} respectively. Similar values were previously ascribed to electrostatic interactions as well as hydrogen bonding between

Table 1
Chemical analysis, chemical formulae, and cell parameters of LDH and LHS samples.

Sample	%Zn[a]	%Cr[a]	%C[a]	%H_2O	Chemical formula	a (Å)	c (Å)	S (m^2/g)
LDH-Cl	36.6(37.0)	14.7(14.2)	<0.1(0)	9.7	$Zn_2Cr(OH)_6Cl{\cdot}1.9\ H_2O$	3.12	23.6	862
LDH-COO	24.8(26.8)	10.0(10.4)	16.5(18.1)	8.5	$Zn_2Cr(OH)_6(R\text{-}COO){\cdot}2.3\ H_2O$	3.10	52.1	616
LDH-SO_3	22.6(25.8)	10.7(10.1)	12.3(14.2)	6.1	$Zn_2Cr(OH)_6(R\text{-}SO_3){\cdot}1.7\ H_2O$	3.09	51.2	591
LHS-Cl	53.0(54.8)	–	<0.1(0)	10.6	$Zn_5(OH)_8Cl_2{\cdot}3.5\ H_2O$	6.33	23.7	700
LHS-COO	37.7(38.6)	–	20.2(19.9)	8.6	$Zn_5(OH)_8(R\text{-}COO)_2{\cdot}4.0\ H_2O$	6.32	56.7	493
LHS-SO_3	39.1(38.3)	–	12.7(15.9)	0.9	$Zn_5(OH)_8(R\text{-}SO_3)_2{\cdot}0.4\ H_2O$	6.19	58.2	464

[a] Between parenthesis, theoretical composition according to the proposed chemical formulae.

equivalent oxygen atom of benzoate carboxylate group and LDH layers [37,38]. For LHS—COO, these bands were registered at 1546 and 1408 cm^{-1} similarly to that obtained for benzoate intercalated LHSs [34], where this value was considered indicative of the anion coordination to Zn^{2+}. The ν_{asym} and ν_{sym} bands shifting to higher wavenumbers suggested a weakening of the C—O bonds of the carboxylate group caused by the anion coordination to Zn^{2+}.

According to the literature [39], sodium benzenesulfonate (NaBS) presents three bands corresponding to the ν_{asym} mode of the SO_3^- group at 1200, 1170 and 1025 and one at 990 cm^{-1} corresponding to the ν_{sym} mode. For LDH—SO_3, only three of these bands were recorded, the first one being obscured by the wide band at 1189 cm^{-1}, which indicated that the sulfonate group symmetry was higher than for NaBS. This observation was consistent with non-directional electrostatic interactions between the layers and the R—SO_3^- anions, concurrent with hydrogen binding between the three oxygen atoms of the SO_3^- group and the hydroxylated layer. On the contrary, all four bands of the SO_3^- group were obtained for LHS—SO_3, indicating that the anion interacted with the solid by only one oxygen atom, indicative of the coordination bonding with the Zn^{2+}. Besides, the band positions were shifted to wavenumbers lower than those of LDH—SO_3, which suggested that, contrarily to R—COO^- anion, R—SO_3^- was more weakly bonded to LHS layers.

The changes in the IR spectral features were stronger for R—SO_3^- than for R—COO^- anion, in good agreement with the higher deformation capacity of sulfonate groups associated to benzyl rings proposed by Fleutot et al. [38]. The rigidity of the carboxylate group was ascribed by these authors to its π conjugation with the benzyl ring, which does not occur for aromatic sulfonates.

3.2. Interfacial characterization

Fig. 2 shows the d and ζ vs. pH curves of both LDH and LHS samples; lines are added as a guide to the eye. Also, autocorrelation curves and intensity size distributions of LDH—Cl and LHS—Cl particles at two pH values are provided as supporting information (Figure S3).

Both curves presented different profiles depending on the solid structure. LDH particles (Fig. 2A) exhibited a positive, almost constant ζ value up to pH 10.5. A ζ decrease occurred at pH > 10.5, leading to an isoelectric point at pH 11. Such behavior was similar to that observed in previous works [5,19] for LDHs intercalated with Cl^-, which exclusively presented electrostatic interactions with the layers. R—COO^- and R—SO_3^- presented no specific interactions such as those producing a particle charge reversal for dodecylsulfate-intercalated Mg–Al LDH [18]. All LDH particles presented a d value (Fig. 2B) around 1 μm in the 6–10 pH range. An increasing particle size was obtained at pH > 10.5 as a result of a diminution in the particle charge and the consequent particle aggregation. These samples presented multimodal distributions at any given pH (Figure S2) and their mean particle size displaced to higher values with increasing pH.

For LHS—Cl, ζ values were near 0 at pH around 8, and increasingly negative values for LHS—COO and LHS—SO_3 (Fig. 2C). The coordination bonding of the interlayer anionsto Zn^{2+} in tetrahedral positions caused a complete screening of the layer charge. Moreover, the chemical affinity of the aromatic anions for the particle surface caused their incorporation in excess to the coordination sites and the negative charging observed for LHS—COO and LHS—SO_3. This chemical affinity was caused by the higher charge density of LHS layers and the π–π stacking interactions enhancement mentioned in Section 3.1. The negative charge was larger for LHS—SO_3 than for LHS—COO, which indicated a higher anion excess in the surface of the former. Similarly to that observed for LDHs, increasing pH values produced an increase in the negative charge of LHS particles in all cases. At pH 8, LHS particles presented a hydrodynamic radius larger than those of LDHs and, as a consequence of the charging dependence on pH, a d decrease with increasing pH (Fig. 2D). The samples showed unimodal size distributions with high polydispersity at pH 8 (Figure S3), decreasing both the polydispersity and the mean particle size with increasing pH.

Both the layer structure and the interlayer anion affected the hydrophilic/hydrophobic character of the solids (Fig. 3 and supporting information, Figure S4). The surface of LDH—Cl was hydrophilic ($\theta = 30 \pm 2^\circ$), in good accord with that obtained in previous works [18]. Higher θ values were obtained for LDH—COO ($\theta = 78 \pm 4^\circ$) and LDH—SO_3 ($\theta = 70 \pm 4^\circ$), agreeing with the presence of the aromatic anions not only in the interlayer space, but also on the particle surface. On the other hand, LHS—Cl presented a higher contact angle ($\theta = 51 \pm 3^\circ$) than LDH—Cl, related to the complete compensation of the layers charge and the weak bonding between water molecules and Cl^- anions coordinated to surface Zn^{2+} [4]. A particularly high θ (=$120 \pm 6^\circ$) value was obtained for LHS—COO, as corresponded to the high surface concentration of aromatic anions and their ordered arrangement. Nevertheless, this θ value was lower than that obtained for a p-aminobenzoate LHS ($\theta = 151^\circ$) by Xing et al. [40]. In the case of LHS—COO, an anion excess was placed on the particle surface, as exposed by its negative ζ value at pH 8 (Fig. 2). Since the coordination sites were all occupied, the anions in excess were disposed in a bilayer disposition, with their polar groups pointing to the aqueous side of the interface and diminishing the surface hydrophobicity, as previously obtained for surfactant intercalated LDHs [11,18]. In good agreement with its more negative ζ value (Fig. 2C), LHS—SO_3 presented a θ value (=$84 \pm 4^\circ$) lower than LHS—COO, due to the incorporation of a larger anion excess.

3.3. Reactivity

In order to study the reactivity of these solids, the dependence of σ_{OH} on pH and NaCl concentration was assessed (Fig. 4). Also, for samples containing R—COO^- and R—SO_3^-, $-\sigma_A$ was determined as a function of pH and σ_{OH} vs. pH curves in NaCl + interlayer anion solutions were obtained (Fig. 5).

σ_{OH} vs. pH curves for LDH-Cl (Fig. 4A) presented a behavior similar to that previously obtained [5,19], namely a simultaneous increase in σ_{OH} and pH and shift to lower σ_{OH} with increasing [NaCl] at any given pH. In previous works [5,19], a model of the LDHs particle surface was proposed to describe this behavior. LDHs structural charge was placed in an internal plane and compensated by anion binding reactions, expressed as:

$$X + A^- = XA^- \quad (2)$$

where X and XA^- denoted neutral, unoccupied sites and negatively charged, occupied sites, respectively, and A^- were anions in solution (Cl^-, R—COO^-, R-SO_3^-, OH^-).

The model also considered additional surface charging by protonation–deprotonation reactions of the layer hydroxide groups, expressed as:

$$Zn_2CrOH + OH^- = Zn_2CrO^- + H_2O \quad (3)$$

where $Zn_2CrOH$and Zn_2CrO^- are protonated (neutral) and deprotonated (negatively charged) variable charge sites, respectively.

The model predicted that, at low pH values, the LDH—Cl surface presented only Zn_2CrOH, XCl^-, and a portion of unoccupied X sites, the latter being responsible for the positive charging of the particles (Fig. 2A). Further, two successive reactions were produced as pH increased [5,19]: (1) Zn_2CrOH deprotonation (Eq. (3)), inducing Cl^- detachment from X sites, and (2) OH^-/Cl^-exchange at X sites. These reactions caused a ζ reversal (Fig. 2A) and the presence of

only XOH^- and $ZnCrO^-$ groups at high pH values. The concentration of Cl^- ions in solution strongly affected the OH^-/Cl^- exchange reaction, the hydroxide anions uptake process being favored at low electrolyte concentrations.

Replacing Cl^- anions by $R—COO^-$ and $R—SO_3^-$ in the interlayer of LDHs produced important changes in the σ_{OH} vs. pH curves (Fig. 4B and C). σ_{OH} was independent of NaCl concentration up to pH 10, while a shift to higher σ_{OH} values with increasing [NaCl] was observed at higher pH values. Some interlayer anion release (squares in Fig. 5A and B) occurred for both samples at the initial pH to adjust the exchange equilibrium position in Cl^- containing aqueous solution. The anion release process was favored with increasing pH and almost overlapped with σ_{OH} at the same NaCl concentration (i.e. $-\sigma_A = \sigma_{OH}$) from pH 9 and pH 10 for LDH—COO and LDH—SO_3, respectively. The amount of anion released was almost constant in a larger pH range for LDH—SO_3 than for LDH—COO indicating the higher affinity of the interlayer anion in the former solid. On the other hand, comparison between the σ_{OH} vs. pH curves in the presence (triangles in Fig. 5A and B) and absence (circles) of the interlayer anion showed lower σ_{OH} in the presence of the aromatic anion in solution, similar to the LDH—Cl behavior upon increasing NaCl concentration (Fig. 4A).

LDH-SO_3 and LDH-COO behavior can be explained with the surface sites and reactions proposed for LDH-Cl. Thus, in pure NaCl solutions at low pH values, LDH—COO and LDH—SO_3 presented only Zn_2CrOH, X-($R—COO^-$) or X-($R—SO_3^-$), and a portion of unoccupied X sites causing the positive ζ (Fig. 2A). Afterwards, deprotonation reactions and OH^- exchange at X sites produced a $-\sigma_A$ increase and

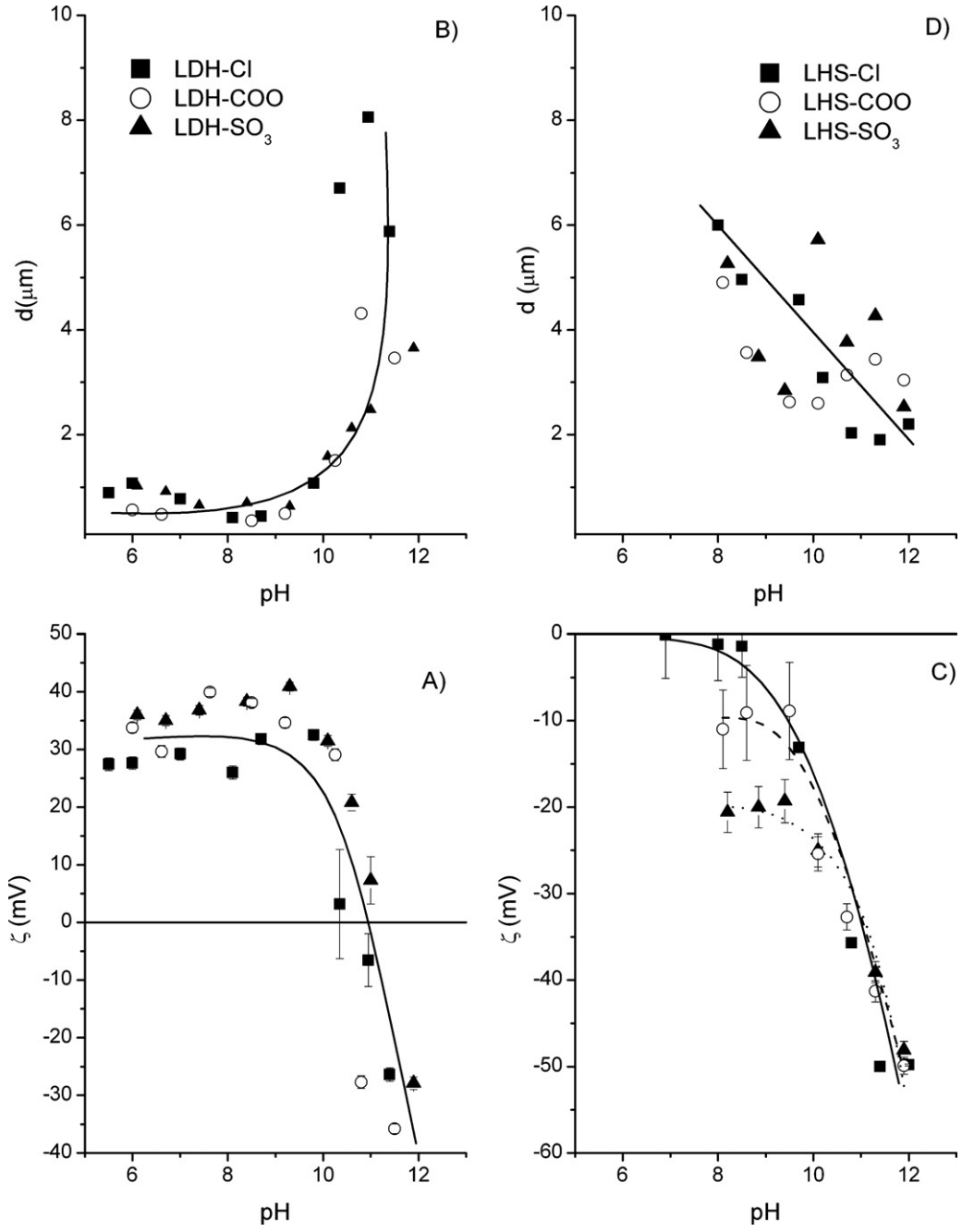

Fig. 2. ζ vs. pH (below) and d vs. pH (above) curves of LDH (left) and LHS (right) samples (0.01 g dispersions in 0.1 L 5×10^{-2} mol L^{-1} NaCl dispersions). Lines were added only as a guide to the eye.

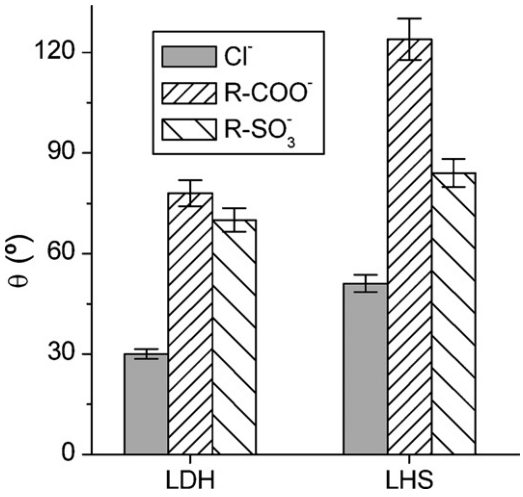

Fig. 3. Water contact angles (θ) of LDH and LHS samples.

the particle charge reversal (Fig. 2A). Finally, complete aromatic anion detachment occurred, leading to XOH^- and $ZnCrO^-$ groups at high pH values. The presence of the aromatic anion in solution, on the other hand, inhibited R—COO^- or R—SO_3^- detachment from X sites and the OH^- exchange reaction. σ_{OH} values for LDH—SO_3 were below those of LDH—COO at any given pH and [NaCl], and R-SO_3^- release started at higher pH value than R—COO^-, confirming that R—SO_3^- had a higher affinity for LDH structure.

LHSs presented quite a different behavior compared to LDHs, particularly when Cl^- was the interlayer anion (Fig. 4). σ_{OH} vs. pH curves of LHS—Cl (Fig. 4D) showed only a small σ_{OH} increase, which augmented parallel to NaCl concentration. Due to the interlayer anion coordinated bonding to Zn^{2+}, no anion detachment reaction (the inverse of Eq. (2)) was possible for LHSs (it would leave the fourth coordination position of Zn^{2+} unoccupied). Hence, only ligand exchange sites, similar to those described for metal oxides

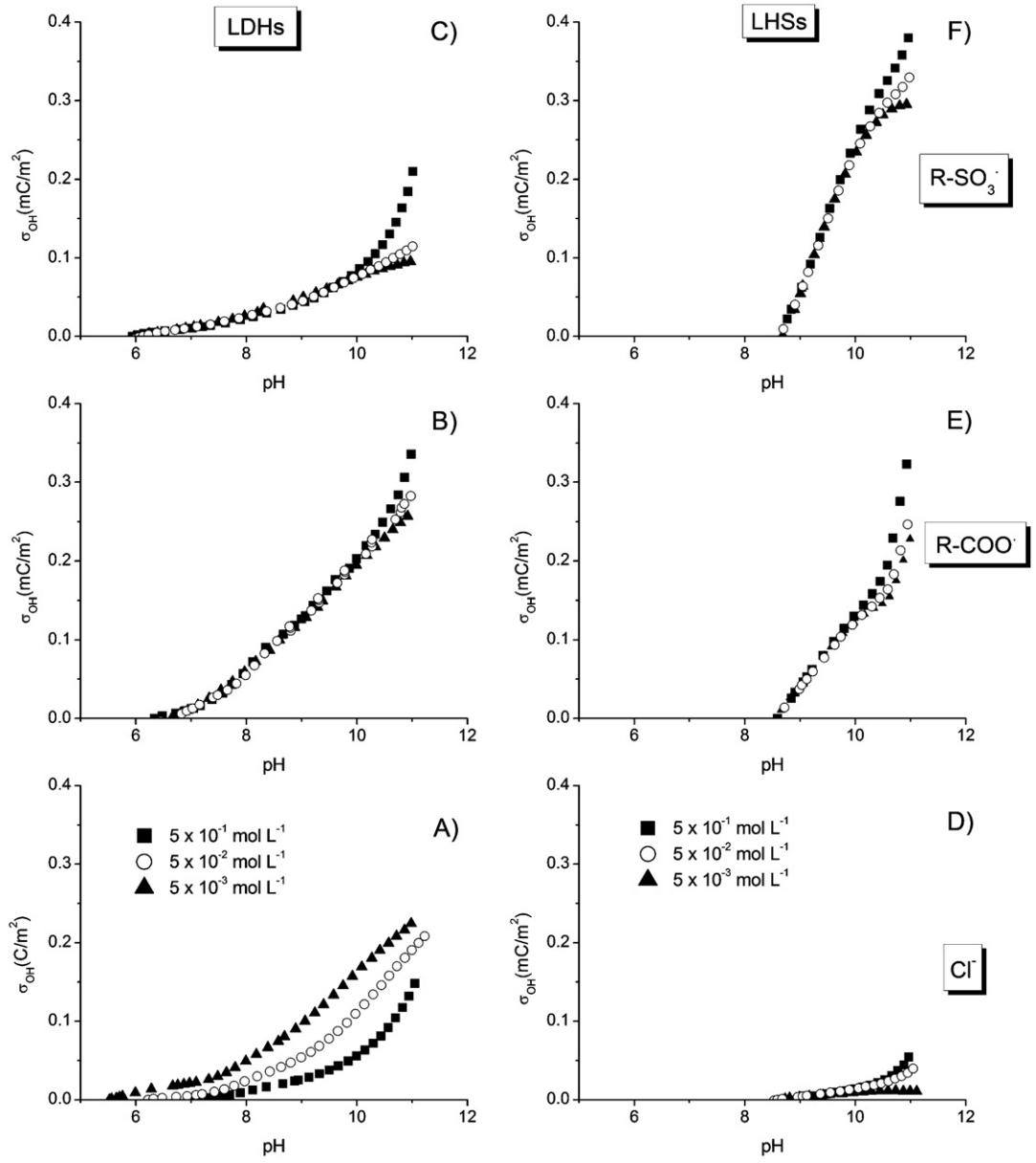

Fig. 4. σ_{OH} vs. pH curves at different NaCl concentrations for (A) LDH-Cl, (B) LDH-COO, (C) LDH-SO_3, (D) LHS-Cl, (E) LHS-COO, (F) LHS-SO_3.

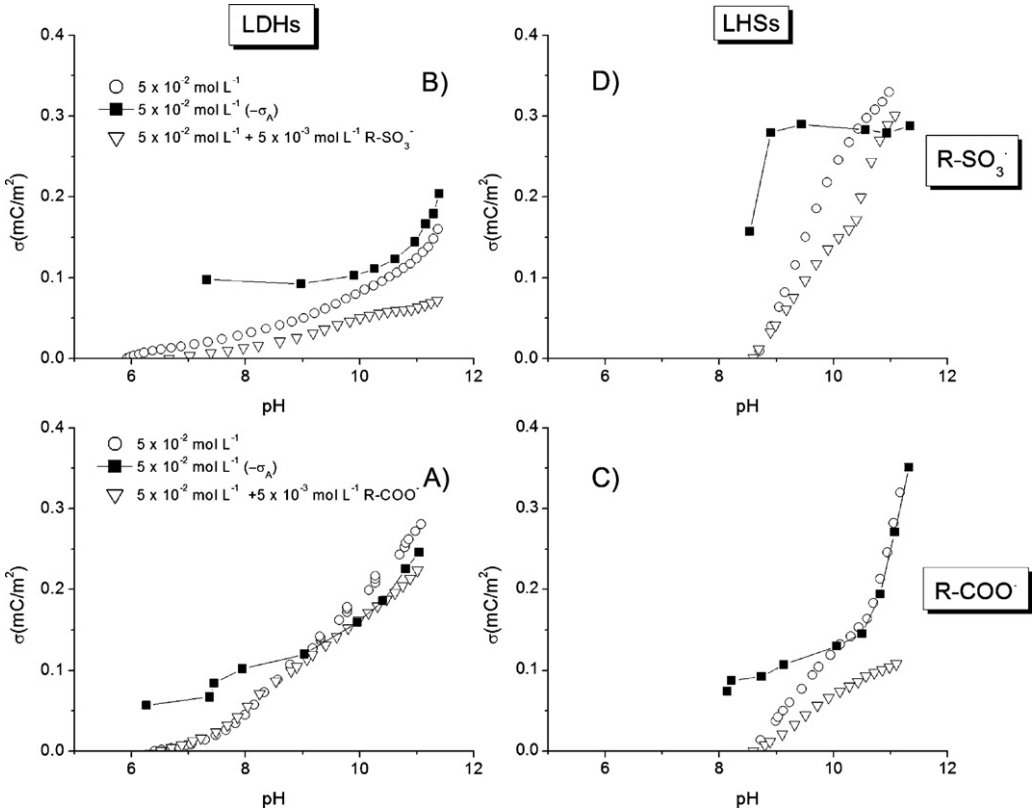

Fig. 5. σ_{OH} vs. pH and $-\sigma_A$ vs. pH curves for: (A) LDH-COO, (B) LDH-SO_3, (C) LHS-COO, C) LHS-SO_3. σ_{OH} vs. pH curves at 5×10^{-2} mol L^{-1} are the same as those presented in Fig. 4 and are included to allow comparison.

[41], were present in these solids. These reactions can be written as follows:

$$(HO)_3 - Zn - A + B = (HO)_3 - Zn - B + A \quad (4)$$

where $(HO)_3$-Zn-A and $(HO)_3$-Zn-B are ligand exchange sites in the solids (note that unoccupied $(HO)_3$-Zn^+ sites are not considered), and A and B are ligands in solution. Depending on the ligand charge, these sites are positively charged or neutral. As Cl^- anions were coordinating Zn^{2+} [42], LHS-Cl particles were neutral at pH 8 (Fig. 2C). Intercalated Cl^- ions were hardly exchanged by OH^- in solution due to the ordered and compact solid structure of this sample [42] and, therefore, $(HO)_3$-Zn-Cl groups were mainly present in the studied pH range. The small σ_{OH} and its dependence on [NaCl] (Fig. 4D) was assigned to deprotonation reactions, responsible for the negative ζ at high pH values (Fig. 2C). Similarly to LDHs, they can be written as follows:

$$Zn_3OH + OH^- = Zn_3O^- + H_2O \quad (5)$$

Nevertheless, this reaction was quite limited as, contrarily to LDHs, no anion detachment could be produced from the solid to compensate the negative charge introduced by Zn_3O^- groups.

On the other hand, LHS—COO and LHS—SO_3 presented ligand exchange reactions with OH^-, as indicated by the higher σ_{OH} (Fig. 4E and F). σ_{OH} showed a steep increase for LHS—SO_3 at pHs lower than 10, while for LHS-COO such an increase was observed at pHs higher than 10. A similar pattern was noticed in $-\sigma_A$ vs. pH curves (Fig. 5C and D). The main $-\sigma_A$ increase was suddenly registered at the beginning of the experiment (pH around 10) for LHS—SO_3 while it was observed at pH > 10 for LHS—COO. Finally, σ_{OH} vs. pH curves in the presence (triangles in Fig. 5C and D) and absence (circles in Fig. 5C and D) of the interlayer anion branched out from low pHs, being the σ_{OH} values lower in the presence of the aromatic anion at any given pH. Also, a displacement of the steep σ_{OH} increase towards higher pH values occurred: out of the registered pH range in the case of R—COO^- anions and to pH 10.5 approximately for R-SO_3^- anions.

The main difference between LHS-Cl and LHS—COO or LHS—SO_3 was the presence of organic anions in excess to the coordination sites, as indicated by the negative ζ values (Fig. 2C) and the contact angle measurements (Fig. 3). R—COO^- was initially removed by Cl^- ions in solution at pH < 10, which produced an initial anion removal, although a slight dissolution of the corresponding solid cannot be discarded [4]. Additionally, hydroxide anions were incorporated by ligand exchange reactions with the aromatic anion (Eq. (4)) at pH values higher than 10 (Fig. 5C: $-\sigma_A = \sigma_{OH}$) up to the complete R—COO^- detachment. As expected, this ligand exchange reaction was inhibited by the addition of R—COO^- in solution, as demonstrated by the σ_{OH} decrease observed in Fig. 5D, while it did not depend on NaCl concentration (Fig. 4E). Deprotonation reactions (Eq. (5)) were also, in this case, responsible for the increasingly negative ζ at high pH values (Fig. 2C).

A significantly different behavior was observed with LHS-SO_3 sample. A high amount of R—SO_3^- was removed by Cl^- ions without consuming OH^- (Fig. 5D) indicating that not only the amount in excess was detached but also R—SO_3^- anions coordinated to Zn^{2+} (Eq. (4)). It is important to note that R—SO_3^- was intercalated in LHS-SO_3 in the presence of approximately the same concentration of Cl^- anions (from the cation salt, see experimental part) indicating that the organic anion presented higher affinity for the layers. However, Cl^- concentration was much higher than the amount of R—SO_3^- in the layers when performing the $-\sigma_A$ vs. pH experiment and displaced the equilibrium position of the ligand exchange reaction (Eq. (4)) towards the removal of the organic anion. In short, the affinity of these two anions for the LHS layers was comparable and the presence of one (or a mixture) of them in the layers was highly dependent on their concentration ratios. Thus, similarly

to that obtained for LHS—COO, the ligand exchange reaction was inhibited by the addition of $R—SO_3^-$ in solution while it did not depend on NaCl concentration (Fig. 4F).

4. Conclusions

The particle charge, hydrophilic character, and hydroxide anions uptake of the LDHs and LHSs were controlled by both layer structure and interlayer anion (Cl^-, $R—COO^-$ and $R—SO_3^-$). Opposite behaviors were achieved with appropriate combinations, which highlight the high customization capacity of these solids. The different anion binding type of each layer structure determined the charging behavior, while the extent and orientation of the anions hydrophobic tails controlled the particle surface hydrophobic/hydrophilic character. The reactivity of the solids was determined by the anion binding type: in the electrostatic interactions in LDHs allow all attachment, detachment and exchange reactions, while only the latter were possible for LHSs due to anion coordination to Zn^{2+}. The interlayer anion ionizable group determined the anion binding strength and consequently the anion/ligand exchange equilibrium of LDHs and LHSs: $R—COO^-$ bonded more strongly to LDHs than $R—SO_3^-$, while the opposite relation was obtained for LHSs.

Acknowledgements

Economic support by SeCyT-UNC, FONCyT, RIARTAS-CYTED, and CONICET is gratefully acknowledged. Thanks to Karina Plasencia for English proofreading.

Appendix A. Supplementary data

Supplementary data associated with this article can be found, in the online version, at http://dx.doi.org/10.1016/j.colsurfa.2012.12.002.

References

[1] D.G. Evans, R.C.T. Slade, in: X. Duan, D.G. Evans (Eds.), Layered Double Hydroxides, Springer-Verlag, Berlin, 2006, p. 1.
[2] F. Wypych, K.G. Satyanarayana (Eds.), Clay Surfaces: Fundamentals and applications, Elsevier, Amsterdam, 2004.
[3] S.P. Newman, W. Jones, J. Solid State Chem. 148 (1999) 26.
[4] G.G.C. Arizaga, K.G. Satyanarayana, F. Wypych, Solid State Ionics 178 (2007) 1143.
[5] R. Rojas, M. Arandigoyen, C. De Pauli, M.A. Ulibarri, M.J. Avena, J. Colloid Interf. Sci. 80 (2004) 431.
[6] U. Costantino, V. Ambrogi, M. Nocchetti, L. Perioli, Microp. Mesop. Mater. 107 (2008) 149.
[7] Z.P. Xu, Q.H. Zeng, G.Q. Lu, A.B. Yu, Engineer. Sci. Chem. 61 (2006) 1027.
[8] R. Rojas, in: A.C. Carillo, D.A. Griego (Eds.), Hydroxides: Synthesis, Types and Applications, Nova Science Publishers, New York, 2012, p. 39.
[9] J. Cornejo, R. Celis, I. Pavlovic, M.A. Ulibarri, Clay Miner. 43 (2008) 155.
[10] Z.P. Xu, Y. Jin, S. Liu, Z.P. Hao, G.Q. Lu, J. Colloid Interf. Sci. 326 (2008) 522.
[11] J. Wang, F. Yang, S. Liu, D. Sun, Langmuir 24 (2008) 10054.
[12] F. Yang, S. Liu, J. Xu, Q. Lan, F. Wei, D. Sun, J. Colloid Interf. Sci. 302 (2006) 159.
[13] F. Bruna, R. Celis, I. Pavlovic, C. Barriga, J. Cornejo, M.A. Ulibarri, J. Hazar. Mater. 168 (2009) 1476.
[14] Z.P. Xu, C.G. Lu, Pure Appl. Chem. 78 (2006) 1771.
[15] Z. Gu, B.E. Rolfe, A.C. Thomas, J.H. Campbell, G.Q. Lu, Z.P. Xu, Biomaterials 32 (2011) 7234.
[16] C. Nyambo, D. Chen, S. Su, C.A. Wilkie, Polym. Degrad. Stabil. 94 (2009) 496.
[17] M.L. Parello, R. Rojas, C.E. Giacomelli, J. Colloid Interf. Sci. 351 (2010) 134.
[18] R. Rojas, F. Bruna, C.P. de Pauli, M.A. Ulibarri, C.E. Giacomelli, J. Colloid Interf. Sci. 359 (2011) 136.
[19] R. Rojas, C. Barriga, C.P. De Pauli, M.J. Avena, Mater. Chem. Phys. 118 (2010) 303.
[20] T. Kameda, T. Yamazaki, T. Yoshioka, Mater. Res. Bull. 245 (2010) 751.
[21] T. Kameda, T. Yamazaki, T. Yoshioka, Solid State Sci. 12 (2010) 946.
[22] M.R. Berber, K. Minagawa, M. Katoh, T. Mori, M. Tanaka, Eur. J. Pharm. Sci. 354.
[23] L.P. Cardoso, R. Celis, J. Cornejo, J.B. Valim, J. Agr. Food Chem. 54 (2006) 5968.
[24] V. Bugatti, G. Gorrasi, F. Montanari, M. Nocchetti, L. Tammaro, V. Vittoria, Appl. Clay Sci. 52 (2011) 34.
[25] M. Herrero, S. Martínez-Gallegos, F.M. Labajos, V. Rives, J. Solid State Chem. 184 (2011) 2862.
[26] J. He, M. Wei, B. Li, Y. Kang, D.G. Evans, X. Duan, in: X. Duan, D.G. Evans (Eds.), Layered Double Hydroxides, Springer-Verlag, Berlin, 2006, p. 89.
[27] G.G.C. Arizaga, A.S. Mangrich, F. Wypych, J. Colloid Interf. Sci. 320 (2008) 238.
[28] S.P. Li, W.H. How, S.H. Han, L.F. Li, W.A. Shao, J. Colloid Interf. Sci. 257 (2003) 244.
[29] H. Roussel, V. Briois, E. Elkaim, A. de Roy, J.P. Besse, J. Phys. Chem. B 104 (2000) 5915.
[30] H. Roussel, V. Briois, E. Elkaim, A. de Roy, J.P. Besse, J.P. Jolivet, Chem. Mater. 13 (2001) 329.
[31] G.G.C. Arizaga, J.E.F.C. Gardolinski, W.H. Schreiner, F. Wypych, J. Colloid Interf. Sci. 330 (2009) 352.
[32] V. Prévot, C. Forano, J.P. Besse, Appl. Clay Sci. 18 (2001) 3.
[33] M. Lakraimi, A. Legrouri, A. Barroug, A. de Roy, J.P. Besse, Mater. Res. Bull. 41 (2006) 1763.
[34] J. Miao, M. Xei, H. Itoh, Q. Feng, J. Mater. Chem. 16 (2006) 474.
[35] F. Wypych, G.G.C. Arizaga, J.E.F.C. Gardoliski, J. Colloid Interf. Sci. 283 (2005) 130.
[36] K. Nakamoto, in: Infrared and Raman Spectra of Inorganic and Coordination Compounds, 4th edn, J. Wiley & Sons, New York, 1986.
[37] Y. Wang, D. Zhang, Mater. Res. Bull. 46 (2011) 1963.
[38] S. Fleutot, H. Martinez, J.C. Dupin, I. Baraille, C. Forano, G. Renaudin, D. Gonbeau, Solid State Sci. 13 (2011) 1676.
[39] L. Pejov, M. Ristrova, Z. Zdravkovski, B. Šoptrajanov, J. Mol. Struct. 524 (2000) 179.
[40] L.L. Xing, B. Yuan, S.X. Hu, Y.D. Zhang, Y. Lu, Z.H. Mai, M. Li, J. Phys. Chem. B 112 (2008) 3800.
[41] C.E. Giacomelli, M.J. Avena, C.P. De Pauli, J. Colloid Interf. Sci. 188 (1997) 387.
[42] F.C. Hawthorne, E. Sokolova, Can. Miner. 40 (2002) 939.